Arabian Journal of Geosciences (2021) 14: 1663
https://doi.org/10.1007/s12517-021-07721-z

ORIGINAL PAPER

Formation mechanism of authigenic chlorite in sandstones of the Middle Jurassic Sha 1 Member in the northeastern central Sichuan Basin, China

Qinming Cao[1] · Zhengxiang Lv[1,2] · Xiang Li[1,2] · Yuanhua Qing[2,3] · Dong Huang[4]

Received: 26 January 2021 / Accepted: 23 June 2021 / Published online: 4 August 2021

Abstract

Using thin sections, scanning electron microscopy, electron probe, X-ray diffraction, and isotopic techniques, the formation mechanisms of authigenic chlorite rims in sandstones of the Middle Jurassic Sha 1 Member in the northeastern central Sichuan Basin are analyzed. Authigenic chlorite has three forms in Sha 1 Member sandstones, grain-coating, pore-lining, and pore-filling; pore-lining chlorite with a double-layer structure is the main type. The grain-coating and inner pore-lining chlorites formed in stage A of eodiagenesis, originating from the hydration and hydrolysis of silicate minerals and the transformation of montmorillonite to chlorite in Fe^{2+}- and Mg^{2+}-rich pore fluids. The outer pore-lining chlorite was deposited from stage B of eodiagenesis to stage A1 of mesodiagenesis and was related mainly to the transformation of montmorillonite to illite and the dissolution of silicate minerals with organic and carbonic acids releasing sufficient Fe^{2+} and Mg^{2+}. The pore-filling chlorite, which was related to the dissolution of silicate minerals by carbonic acid from decarboxylation of organic acid and transformation of clay minerals (such as illite) to chlorite, formed mainly in phase A2 of mesodiagenesis. Fe and Mg for the authigenic chlorites mainly originated from dissolution of magmatic lithic debris and biotite rich in these elements and compaction fluids from the surrounding mudstones. The authigenic chlorites are mainly distributed in medium- and fine-grained sandstones of shallow lake beach bar, estuary bar, and subaqueous distributary channel microfacies.

Keywords Central Sichuan Basin · Reservoir · Pore-lining · Chlorite · Shaximiao Formation · Formation mechanism

Introduction

As a common mineral in clastic rocks, authigenic chlorite has important influences on the preservation of primary pores and the quality of reservoirs in middle-deep clastic rock reservoirs (AliKhoudja et al. 2020; Pittman and Lumsden 1968; Xia et al. 2020; Virolle et al. 2019). Research on the origin of authigenic chlorite and its contribution to the preservation of sandstone primary pores began in the 1950s (Heald 1950; Heald and Anderegg R 1960). Research on chlorite has always been a popular topic in the field of clastic diagenesis and reservoir prediction (Branimir et al. 2020). However, the formation mechanism of authigenic chlorite remains controversial (Lan 2011). Current research focuses on exploring the sources of Fe and Mg (Grigsby 2001; Huang et al. 2004). The chlorite formation modes can be summarized as clay mineral transformation, direct precipitation from pore fluid, and clastic particle alteration (Gould et al. 2010; Bahlis and De Ros 2013; Worden et al. 2020).

Authigenic chlorite rims have dual effects on reservoir development. The negative effects include plugging pores and throats and reducing reservoir quality (Zhou et al. 2020). Most scholars believe that the authigenic chlorite rims represent constructive diagenesis. The positive roles of authigenic chlorite rims include the inhibition of compaction (or pressure

Responsible Editor: Domenico M. Doronzo

✉ Zhengxiang Lv
lvzhengxiang13@cdut.cn

[1] State Key Laboratory of Oil-Gas Reservoirs Geology and Exploitation, Chengdu University of Technology, Chengdu 610059, China

[2] College of Energy Resources, Chengdu University of Technology, Chengdu 610059, China

[3] School of History, Geography and Tourism, Chengdu Normal University, Chengdu 611130, China

[4] Institute of Exploration and Development, PetroChina Southwest Oil & Gasfield Company, Chengdu 610041, China

solution) (Xie et al. 2010), inhibition of quartz overgrowth (Ehrenberg 1993; Pittman et al. 1992), promotion of dissolution (Liu et al. 2009), and transition of rock wettability, which benefit oil and gas accumulation (Alotaibi et al. 2011; Mahmoud and Mohamed 2018). The main controversies are as follows: (1) There are different opinions on the mechanism by which chlorite rims inhibit quartz overgrowth, although it is generally believed that chlorite prevents authigenic quartz from nucleating on the surface of detrital quartz (Line et al. 2018; Sun et al. 2014). (2) Chlorite rims can improve the anti-compaction ability of sandstone (Huggett et al. 2015; Anjos et al. 2009); however, some scholars point out that chlorite rims have low hardness and intergranular porosity and that their compaction resistance is limited (Xiang et al. 2016).

Mechanical compaction and authigenic mineral filling are the two main factors for sandstone densification in the Middle Jurassic Sha 1 Member in the central Sichuan Basin (Dowey et al. 2012; Yang et al. 2016). Chlorite is the main authigenic clay mineral in sandstones of the Sha 1 Member. The formation of high-quality reservoirs is closely related to the development of chlorite rims. However, there has been no systematic analysis of the formation mechanism for authigenic chlorite. Some scholars briefly described the characteristics of authigenic chlorite in the Sha 1 Member of the Shaximiao Formation in the central Sichuan Basin and considered authigenic chlorite to have a positive impact on the reservoir (Zhang 2013; Zhao et al. 2010), but their research did not address the formation mechanism. This study mainly uses petrology, mineralogy, and geochemistry to deeply analyze the occurrence state, material source, and formation mechanism of authigenic chlorite in the Sha 1 Member of the Middle Jurassic Shaximiao Formation in the northeastern Sichuan Basin, to provide the basis for predicting the distribution of relatively high-quality reservoirs in sandstones.

Geological setting

The Sichuan Basin is located in southwestern China, with the Longmenshan orogenic belt to the west, the Micangshan uplift belt and Dabashan uplift belt to the north, the Xuefengshan intercontinental tectonic deformation system to the southeast, and the Emeishan-Liangshan fold belt to the southwest (Fig. 1). The Central Sichuan area is a stable area in the central part of the Sichuan Basin, with weakly developed faults and gentle stratigraphic dips (dip angles of 2–5°); the large slope gradually decreases from south to north (Zhang 2103). The study area is located in the northeastern part of the central Sichuan Basin (Fig. 1). The Shaximiao Formation (J_2s) in the central Sichuan Basin is divided from bottom to top into the Sha 1 Member (J_2s^1) and Sha 2 Member (J_2s^2) (Fig. 2). The Sha 1 Member is mainly a set of lake-delta sedimentary systems, and the Sha 2 Member is mainly a set of river flood plain sedimentary systems. The oil in the Shaximiao Formation is generated mainly from the dark mudstone of the underlying Liangshan Formation (J_1l), and the reservoir type is typical continuous sandstone reservoir (Chen et al. 2005).

Materials and methods

Sixty-nine blue epoxy-impregnated thin sections from 16 exploration wells in the study area were selected for petrographic and diagenetic analyses. The thin sections were partly stained with alizarin red for carbonate mineral determination. Point counting with at least 400 points per thin section was performed by using a Leica DM4500P polarizing microscope to analyze the rock mineralogy, diagenetic relationships, porosity characteristics, and clay growth occurrence in the reservoir spaces.

A Quanta 450 FEG scanning electron microscope was used to identify minerals and mineral occurrence relationships. Moreover, some minerals that were difficult to identify were analyzed semiquantitatively with an SDD Inca X-Max 50 energy spectrometer.

Some typical samples were analyzed quantitatively with an EPMA-1720Hseries electron microprobe to identify mineral types and chemical compositions. Twenty-five sandstone samples were selected for X-ray diffraction analysis, a semi-quantitative method, to obtain the mineral assemblage of the whole rock. Clay minerals were separated from the same twenty-five sandstone samples by the natural sinking method, and their relative contents were measured through X-ray diffraction analysis.

Based on the results of petrological and mineralogical studies mentioned above, samples with authigenic carbonate cements were chosen to analyze carbon and oxygen isotope values. In situ carbon and oxygen isotope analysis was performed using a Nd:YAG laser microprobe. For isotopic analysis, laser probe microsampling of C and O from carbonate cements was achieved by focusing a laser beam, with a wavelength of 1064 nm and a diameter of 20 μm, onto a sample situated in a vacuum chamber to ablate a small area on the sample and liberate CO_2 gas. CO_2 gas was injected directly into a MAT253 stable isotope mass spectrometer for isotope analysis with an accuracy ≤0.02/‰ according to the industry standard (SY/T 5238-2008) (Li et al. 2008).

Thirty-one core samples were selected from 8 exploration wells for reservoir property studies (Table 1). The properties, including porosity, permeability, and density, were measured by an STL-IV core permeability tester and an HXK-III helium porosity automatic tester.

All the above experiments were completed at the State Key Laboratory of Oil and Gas Reservoir Geology and Development Engineering, Chengdu University of Technology, Chengdu, China.

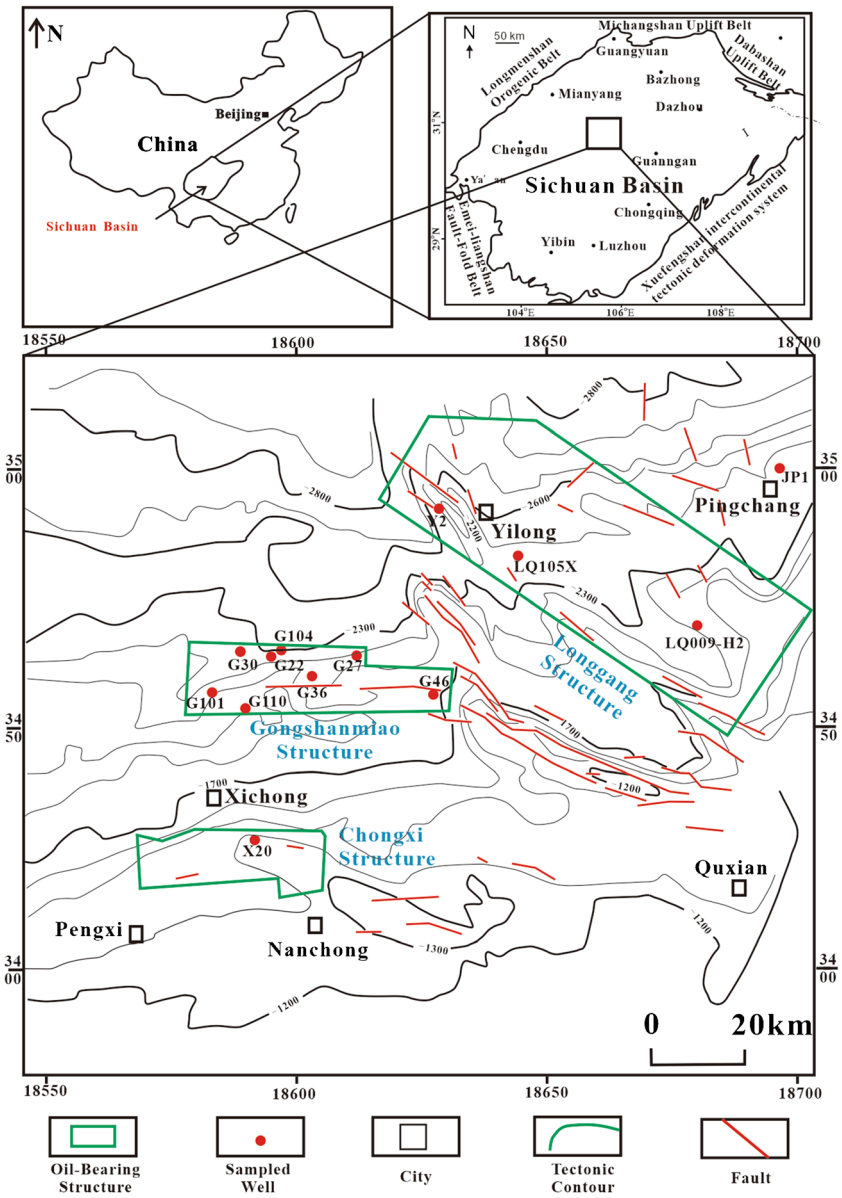

Fig. 1 Locations of the study area and the critical sampling wells

The Institute of Exploration and Development of PetroChina Southwest Oil & Gasfield Company provided some of the data in this study, including mud logging, wireline logging, and organic geochemical data such as vitrinite reflectance (Ro).

Results

Reservoir petrology

The reservoir rock types of the Sha 1 Member are mainly feldspathic litharenite, litharenite, and lithic arkose (Fig. 3a). Whole-rock X-ray diffraction analysis shows that the feldspar clasts are mainly plagioclase (30~59%, average 42%), with a small amount of potassium feldspar (0~17%, average 5.2%) (Table 2). X-ray diffraction analysis of clay minerals (Table 2) indicates that the main clay minerals are chlorite (35~89%, average 68.6%), followed by illite (10~24%, average 24.6%) and small amounts of kaolinite, montmorillonite and mixed-layer clay minerals (Table 2). The particle sizes are mainly fine and medium. The sandstone is characterized by moderate roundness, good sorting, line contacts, and porous cements (Fig. 3b). The sandstones in the Sha 1 Member of the Shaximiao Formation have low compositional maturity and medium structural maturity.

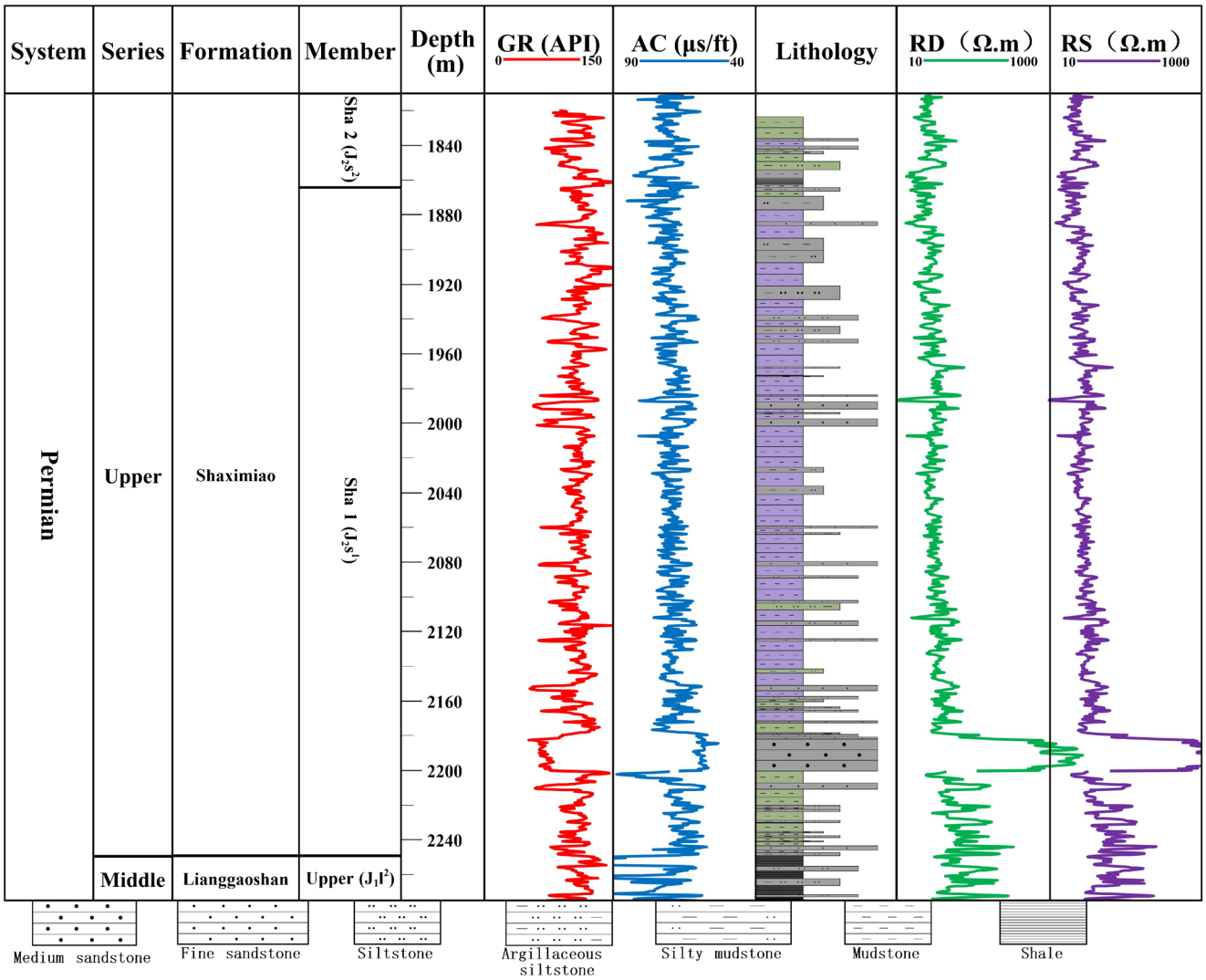

Fig. 2 Composite column of the Shaximiao Formation (well G36)

Sandstone reservoir characteristics

Physical characteristics

Based on the analysis of 31 core plugs sampled from Sha 1 Member sandstones, the porosity can be concluded to vary mainly from 2 to 6%, with porosity greater than 2% accounting for 74% of the total (Fig. 4a). The permeability mostly varies from 0.01 to 1 mD, with permeabilities greater than 0.01 mD accounting for 83% of the observations (Fig. 4b). The sandstone reservoir of the Sha 1 Member has ultralow porosity and ultralow permeability (Ren et al. 2011).

Reservoir space characteristics

The reservoir space of the Sha 1 Member mainly consists of residual primary intergranular pores, intergranular dissolved pores, and intragranular dissolved pores (Fig. 5a, b, c, d, e). In addition, clay minerals (such as kaolinite) develop many intercrystalline pores (Fig. 5f). The remaining primary intergranular pores are mostly triangular in shape (Fig. 5a, c, e) and appear to be always associated with authigenic chlorite rims (Fig. 5a, e). Secondary dissolution pores mostly originate from the dissolution of feldspar particles, which indicates that the rock has experienced intense dissolution (Fig. 5b, d).

Characteristics of authigenic chlorite occurrences

According to the arrangements of chlorite crystals and their contact relationships with particles, there are three modes of authigenic chlorite occurrences in the sandstones of the Sha 1 Member. (1) Grain-coating chlorite (thickness less than 4 μm; Fig. 6a, b). Fine flake-shaped crystals grow perpendicular or oblique to the surfaces of particles and cover the entire grain or most of the grain. Chlorite crystals (thickness less than 1 μm) are distributed parallel to the particles at the contact area due to

Table 1 Sampling information for the Sha 1 Member samples analyzed in the physical property experiment

Well	Depth (m)	Formation	Lithology	Sample length (cm)	Sample diameter (cm)
G104	2529.89	J_2s^1	Brown gray oil soaked fine sandstone	5.174	2.525
G104	2472.87	J_2s^1	Gray fine siltstone	5.147	2.525
JP1	3288.06	J_2s^1	Light gray coarse sandstone	5.144	2.525
JP1	3279.22	J_2s^1	Light gray coarse medium sandstone	5.12	2.525
G36	2243.38	J_2s^1	Light gray fine sandstone	5.17	2.525
G36	2208.84	J_2s^1	Light gray fine sandstone	5.125	2.525
G36	2206.77	J_2s^1	Light gray fine sandstone	5.118	2.525
G46	2196.6	J_2s^1	Light gray fine siltstone	5.087	2.525
G46	2194.66	J_2s^1	Light gray fine sandstone	5.164	2.525
G46	2188.02	J_2s^1	Light gray fine sandstone	5.1	2.525
Y2	2909.96	J_2s^1	Gray fine sandstone	5.017	2.525
X20	1606.58	J_2s^1	Light gray medium fine sandstone	5.186	2.525
X20	1607.78	J_2s^1	Light gray medium fine sandstone	5.022	2.525
X20	1608.88	J_2s^1	Light gray fine sandstone	5.164	2.525
X20	1613.19	J_2s^1	Light gray fine sandstone	5.102	2.525
X20	1613.69	J_2s^1	Light gray fine sandstone	5.309	2.525
X20	1614.94	J_2s^1	Light gray medium fine sandstone	5.081	2.525
X20	1615.87	J_2s^1	Light gray medium fine sandstone	4.953	2.525
X20	1616.97	J_2s^1	Light gray fine sandstone	5.38	2.525
X20	1617.57	J_2s^1	Light gray fine sandstone	5.287	2.525
X20	1618.04	J_2s^1	Greenish gray fine sandstone	5.166	2.525
X20	1618.56	J_2s^1	Greenish gray fine sandstone	5.277	2.525
X20	1618.83	J_2s^1	Greenish gray fine sandstone	5.247	2.525
X56	1650.3	J_2s^1	Light gray fine siltstone	5.26	2.525
LQ105X	3066.47	J_2s^1	Light gray fine sandstone	5.202	2.525
LQ009-H2	2618.69	J_2s^1	Greenish gray fine sandstone	5.135	2.525
LQ009-H2	2625.68	J_2s^1	Greenish gray fine sandstone	5.218	2.525
LQ009-H2	2629.23	J_2s^1	Greenish gray fine sandstone	5.147	2.525
LQ009-H2	2631.6	J_2s^1	Light gray fine sandstone	5.251	2.525
LQ009-H2	2633.65	J_2s^1	Light gray fine sandstone	5.193	2.525
LQ009-H2	2636.45	J_2s^1	Gray fine sandstone	5.522	2.525

compression (Fig. 6b). (2) Pore-lining chlorite (Fig. 6c, d, g, i, j). The pore-lining chlorite has a double-layer structure (Fig. 6c) and is the most widely distributed. The crystal shape and arrangement of the inner pore-lining chlorite (thickness less than 4 μm) are similar to those of the grain-coating chlorite. The outer pore-lining chlorite has large subhedral (or euhedral) leaf-shaped crystals (5–12 μm in diameter) and grows perpendicular to the surface of the particle or the surface of the grain-coating chlorite. The thickness of the outer pore-lining is the same as the crystal diameter, and the crystals cross each other in a honeycomb shape. (3) Pore-filling chlorite (Fig. 6c, h, j, k, l). Pore-filling chlorite fills the intergranular pores with euhedral crystal (3–14 μm in diameter) aggregates (such as rosettes) (Fig. 6l) or dispersed monomers (Fig. 6h). The crystal growth direction is not related to the particle surface. The chlorite rim contains grain-coating chlorite and pore-lining chlorite, with thicknesses of 6–18 μm (mostly 8–15 μm). The thickness of a chlorite rim decreases near the particle contact area.

Chemical composition of authigenic chlorite

According to electron probe and energy spectrum analysis results, the authigenic chlorites in the Sha 1 Member sandstones are all iron-rich chlorites (Table 3). The ratios of FeO/(FeO+MgO) range from 0.59 to 0.78 with an average of 0.67, which is significantly higher than that of standard chlorite (0.59) (Table 3). There are obvious variations in chemical composition among different occurrences of authigenic chlorite. The contents of SiO_2 in grain-coating chlorite and inner pore-lining chlorite are greater than those in outer pore-lining chlorite and pore-filling chlorite.

Table 2 Statistical summary of XRD results (absolute values %)

Well	Depth (m)	Whole rock (%)						Clay (%)				
		Quartz	Potash feldspar	Plagioclase	Calcite	Laumontite	Clay	Montmorillonite	Illite	Kaolinite	Chlorite	Smectite mixed layer
G104	2529.89	48		47			5		17	27	56	
G30	2515.4	33		52	7		8	39	10		51	
G36	2186.27	28	14	41		9	7		25		75	
G36	2191.68	29	17	37		10	7	3	29		68	
G36	2193.75	30	10	31	2	18	10		20		80	
G36	2198.81	40	11	42			7	2	22		77	
LQ009-H2	2618.69	34	5	32	2	20	6		32		68	
LQ009-H2	2625.68	35		51			14		28		66	6
LQ009-H2	2628.31	34	6	39	2	10	9		35		65	
LQ009-H2	2629.23	22	5	36	2	27	7		38		62	
LQ009-H2	2631.6	37		46	4		13		16		76	8
LQ009-H2	2634.72	34		53	2		11		14		72	14
LQ009-H2	2636.45	32	9	50			9		65		35	
LQ009-H2	2638.87	39		47			14		17		74	9
LQ105X	3064.95	52		30	6		12		37		51	12
LQ105X	3066.47	45		35	12		8		46		45	9
X20	1606.58	41	10	40	4		4		21		79	
X20	1613.19	38	10	42			10		16		84	
X20	1613.69	38	8	46			8		13		87	
X20	1614.94	46	7	40	1		6		17		83	
X20	1615.87	53	6	34	1		7		15		85	
X20	1617.57	46	7	32		11	4		11		89	
X20	1618.83	51		45	1		3		20		80	
Y2	2909.96	28		59	2		11		26		38	36

In contrast, the contents of MgO and FeO in grain-coating chlorite and inner pore-lining chlorite are lower than those in outer pore-lining chlorite and pore-filling chlorite (Fig. 7), which indicates their different origins.

Temperature of calcite cementation

Using the average value ($\delta^{18}O_{V\text{-}PDB}$= −10.48‰) of laser oxygen isotopes for well-preserved shells in two mudstone

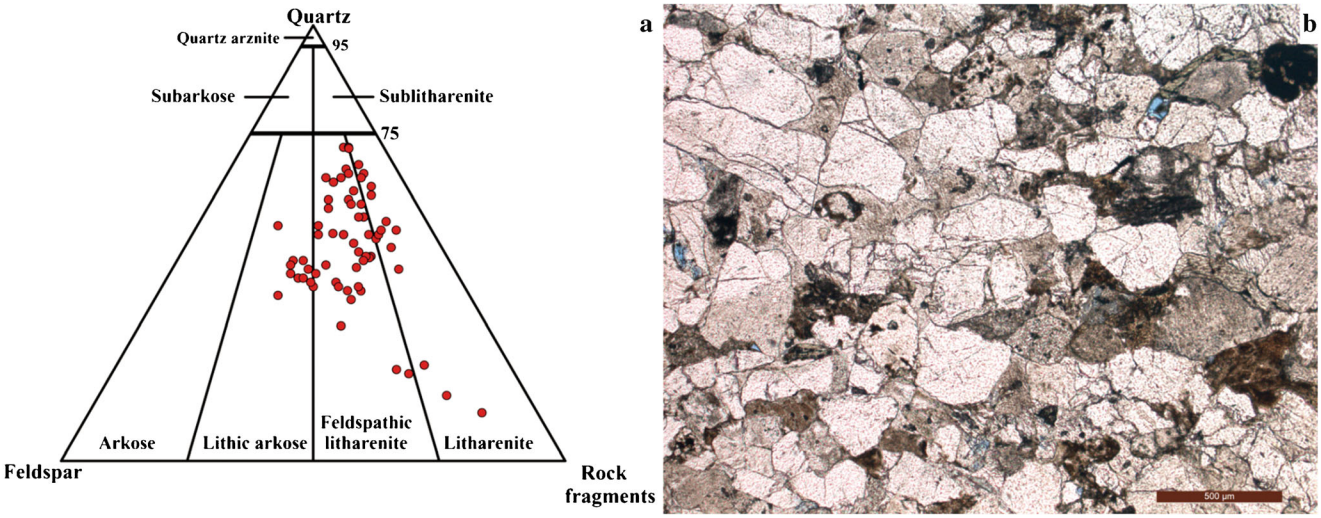

Fig. 3 Characteristics of detrital composition and structure in Sha 1 Member reservoirs. **a** Reservoir rock composition. **b** Photomicrograph showing good sorting, subrounded grains, and line contacts between particles, well G36, 2197.35 m, plane-polarized light (PPL)

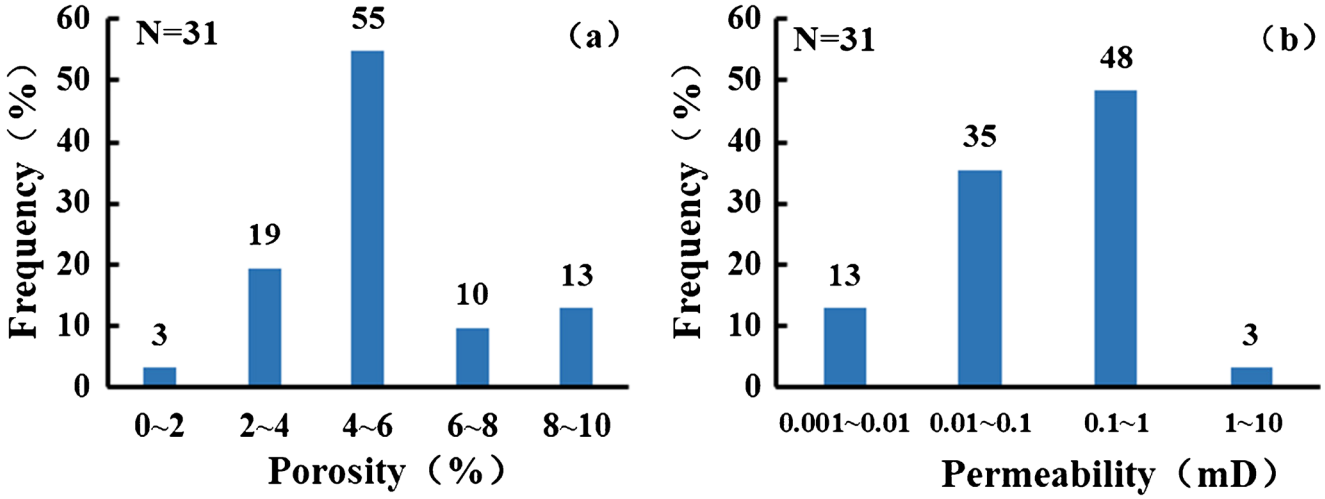

Fig. 4 Porosity and permeability of the Sha 1 Member. **a** Porosity distribution. **b** Permeability distribution

samples from the Sha 1 Member, $\delta^{18}O_{V\text{-}SMOW}$ (−8.49‰) of the early diagenetic fluid is calculated by the calcite-water fractionation equation (Warren, 2000) (assuming a paleosurface temperature of 25°C) and yields a value close to $\delta^{18}O_{V\text{-}SMOW}$ (−8.70‰) of the modern meteoric water in the Sichuan Basin (Lin and Pan 2001). In the middle and late stages, the $\delta^{18}O$ of the diagenetic fluid increased due to oxygen isotope exchange with the surrounding rock (Yuan et al. 2016). Therefore, $\delta^{18}O_{V\text{-}SMOW}$ of the mid-late diagenetic fluid can be replaced by the median value of $\delta^{18}O_{V\text{-}SMOW}$ (−5‰) of the current Jurassic formation water $\delta^{18}O_{V\text{-}SMOW}$ in the Sichuan Basin (Li and Qin 2012). Calculated according to the above fractionation equation, the temperature of authigenic calcite formation was 42.3~122.3°C (Table 4).

Diagenetic fluid salinity

According to the calculation formula for the paleo-salinity index (Z) (Keith and Weber 1964) proposed by Keith and Weber (1964) and the fitting equation for the $\delta^{18}O$ value

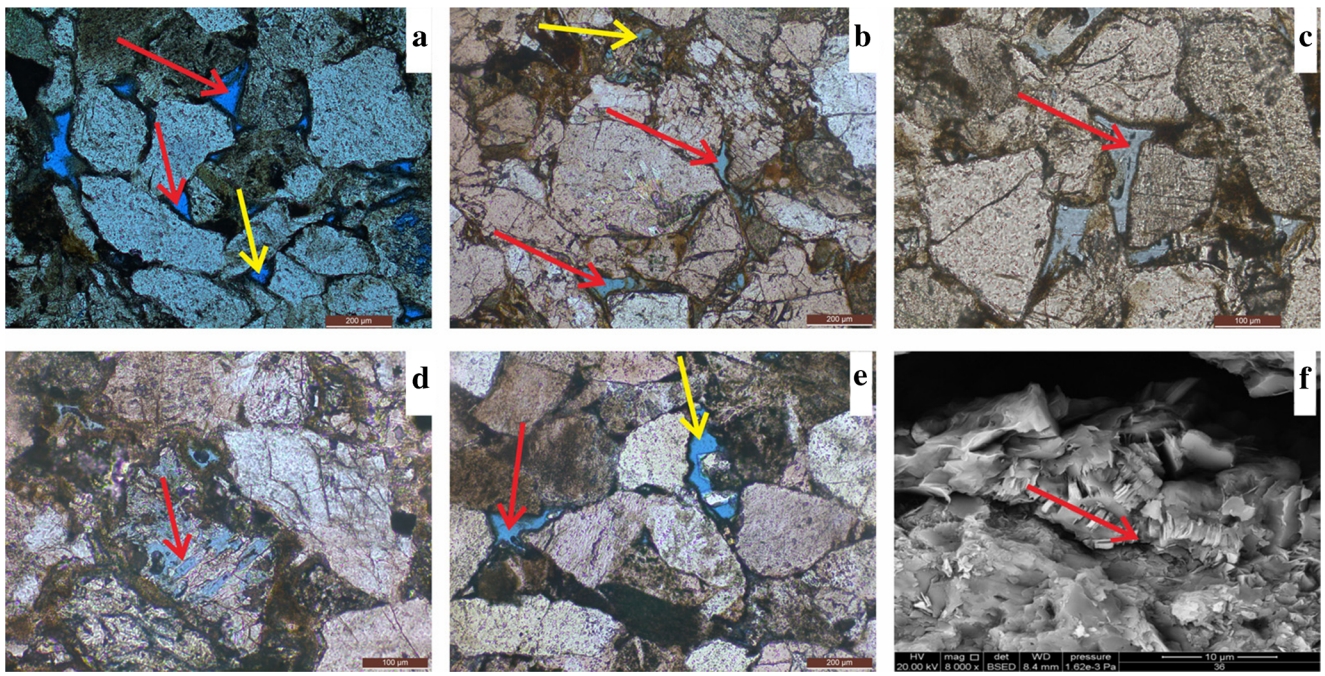

Fig. 5 Reservoir space types of the Sha 1 Member of the Shaximiao Formation. **a** Residual intergranular pores (red arrows) and intergranular dissolved pore (yellow arrow), well X20, 1614.94 m, J_2s^1, PPL. **b** Intergranular dissolved pores (red arrows) and intragranular dissolved pore (yellow arrow), well G104, 2528.66 m, J_2s^1, PPL. **c** Residual intergranular pores (red arrow), well G36, 2186.27 m, J_2s^1, PPL. **d** Intragranular dissolved pore (red arrow), well G46, 2195.25 m, J_2s^1, PPL. **e** Residual intergranular pore (red arrow) and intergranular dissolved pore (yellow arrow), well X20, 1606.58 m, J_2s^1, PPL. **f** Intercrystalline pores in kaolinite, well G101, 2465.5 m, J_2s^1, scanning electron microscopy (SEM)

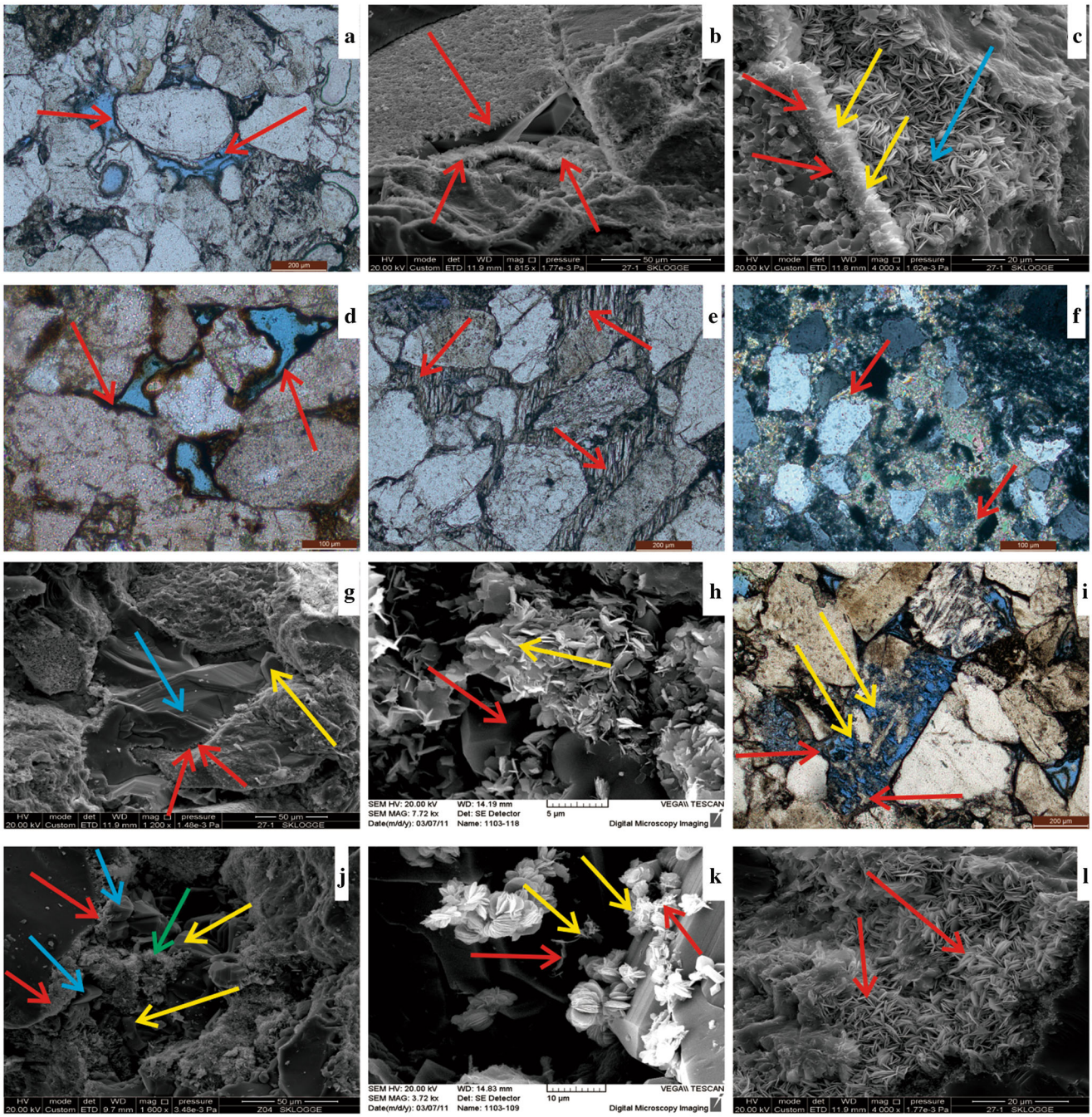

Fig. 6 Occurrence modes of authigenic chlorites. **a** Grain-coating chlorite (red arrows) encases quartz particles, well X20, 1617.57 m, J_2s^1, PPL. **b** Grain-coating chlorite (red arrow), well G27, 2467.15 m, J_2s^1, SEM. **c** From particle edge to pore, the order is inner pore-lining chlorite (red arrows)→outer pore-lining chlorite (yellow arrow)→pore-filling chlorite (blue arrow), well G27, 2467.15 m, J_2s^1, SEM. **d** Well-developed pore-lining chlorite (red arrows) and well-developed primary intergranular pores, well G104, 2530.1 m, J_2s^1, SEM. **e** Pore edges (red arrows) filled with intergranular laumontite and no chlorite rim, well X20, 1617.57 m, J_2s^1, SEM. **f** Pore edges (red arrows) filled with intergranular calcite and no chlorite rim, well G110, 2428.23 m, J_2s^1, cross-polarized light (CPL). **g** Pore-lining chlorite (red arrows) →quartz overgrowth (yellow arrow) →pore-filling quartz (blue arrow), well G27, 2467.15 m, J_2s^1, SEM. **h** Pore-filling quartz (red arrow) →leaf-shaped pore-filling chlorite (yellow arrow), well G36, 2187 m, J_2s^1, SEM. **i** Strongly dissolved feldspar (yellow arrows) with authigenic chlorite rims (red arrows), well X20, 1613.69 m, J_2s^1, PPL. **j** Chlorite rim (red arrows) →quartz overgrowth (blue arrow) →pore-filling quartz (yellow arrows) →pore-filling chlorite (green arrow), well JP1, 3279.22-3279.32 m, J_2s^1, SEM. **k** Intergranular illite (red arrows) transformed into leaf-shaped pore-filling chlorite (red arrow), well G22, 2475.9 m, J_2s^1, SEM. **l** Rose-shaped pore-filling chlorite, well G27, 2467.15 m, J_2s^1, SEM

and salinity (S) of the Pacific Ocean water proposed by Epstein (1953) Yin and Ni (2009), the values of Z and S are calculated (Table 4). The paleo-salinity index Z of the basal cementing calcite in the Sha 1 Member sandstones varies from

Table 3 Chemical composition of different occurrences of authigenic chlorite

Well	Depth (m)	Occurrence	Chemical composition									
			Na_2O	MgO	Al_2O_3	SiO_2	K_2O	CaO	TiO_2	Cr_2O_3	MnO	FeO	NiO
X20	1613.19	Pore-lining chlorite	0.29	9.94	24.95	29.51	0.27	0.21	0.02	0.16	0.67	33.95	0.02
X20	1613.19	Pore-lining chlorite	0.09	9.93	24.30	30.00	0.04	0.25	0.00	0.15	0.70	34.53	0.01
X20	1613.19	Pore-filling chlorite	0.07	9.89	24.43	30.21	0.05	0.28	0.04	0.14	0.69	34.16	0.03
G36	2189.81	Inner pore-lining chlorite	6.43	5.90	13.78	64.23	0.64					9.01	
G36	2189.81	Inner pore-lining chlorite; poorly crystalline	0.00	8.73	8.87	68.03	0.00					14.36	
G27	2467.15	Outer pore-lining chlorite; well-crystallized	0.00	16.50	18.83	39.62	0.00					25.04	
G27	2467.15	Pore-filling chlorite; well-crystallized	0.00	17.22	19.10	38.63	0.00					25.05	
G36	2186.27	Grain-coating chlorite; poorly crystalline	0.00	10.41	10.27	63.91	0.00					15.42	
G46	2195.25	Pore-filling chlorite; well-crystallized		15.16	14.20	35.12	0.00					35.52	

Note: For well X20, the data were obtained from electron probe analysis; for wells G27, G36, and G46, the data were obtained from energy spectrum analysis

64.8 to 128.5 (average 105.1), and the salinity (S) values are between 4.2 and 12.2‰ (average 8.3‰) (Table 4). The early diagenetic fluid was equivalent to saline freshwater, which is basically consistent with the moderately dry and hot climate in the northeastern part of the central Sichuan area during the mid-Jurassic (Zhang 2013). Therefore, authigenic chlorite was difficult to precipitate from the pore fluids.

Discussion

Formation period of authigenic chlorite

The grain-coating chlorite was deposited during the stage when detrital particles were not in contact (Fig. 6a), so it formed the earliest. The pore-lining chlorite formed after the point contact (or line contact) period (Fig. 6d). The inner pore-lining chlorite formation period was equivalent to that of the chlorite coating. The pore-filling chlorite developed later than the outer pore-lining chlorite (Fig. 6c). According to the occurrence characteristics and formation temperatures of various minerals, the formation periods of authigenic chlorite are determined. In the same sections, the area where chlorite rims developed coexists with an undeveloped area rich in laumontite, which implies that the pore-lining chlorite formed after laumontite (Fig. 6a, d). The initial formation temperature of laumontite is generally higher than 50°C (Iijima 2001), and the lowest formation temperature of calcite is 40 °C. Therefore, the temperature of pore-lining chlorite formation was more than 50°C. The quartz overgrowths are located on

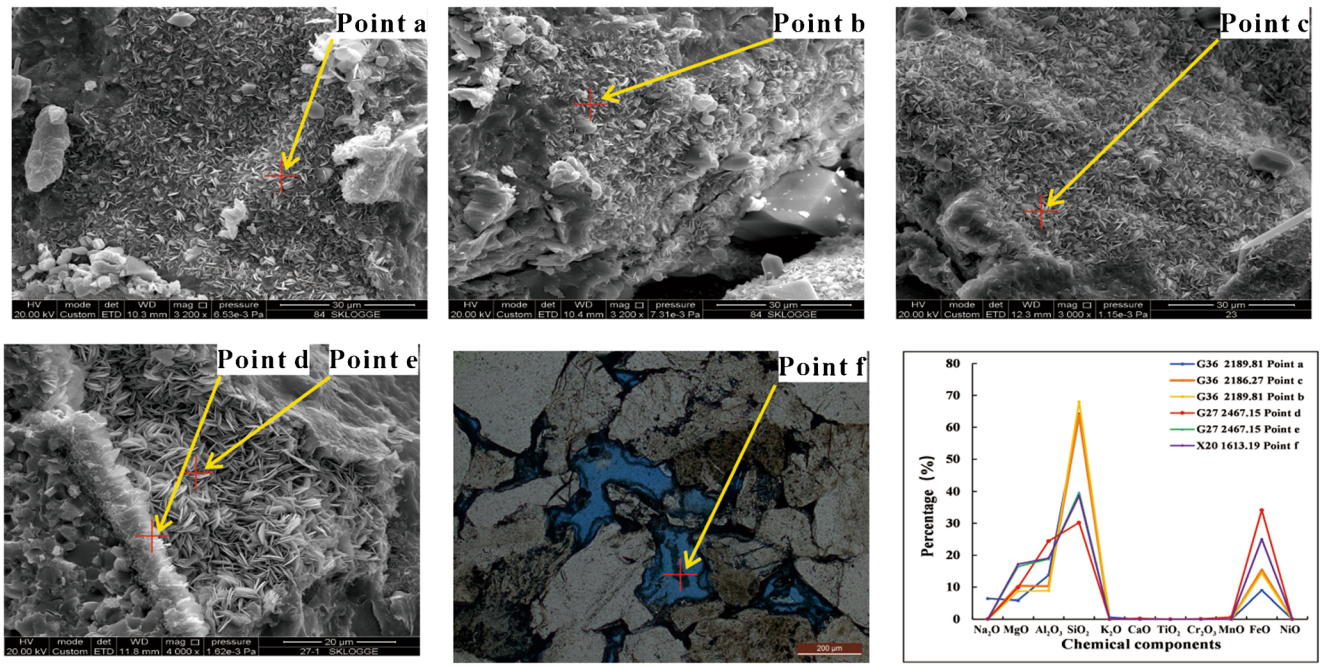

Fig. 7 Chemical composition of different occurrences of authigenic chlorite. **a** Poorly crystalline inner pore-lining chlorite, well G36, 2189.81 m, J_2s^1, SEM. **b** Poorly crystalline pore-lining chlorite, well G36, 2186.27 m, J_2s^1, SEM. **c** Poorly crystalline grain-coating chlorite, well G36, 2189.81 m, J_2s^1, SEM. **d** Well-crystallized outer pore-lining chlorite, well G27, 2467.15 m, J_2s^1, SEM. **e** Well-crystalized pore-filling chlorite, well G27 2467.15 m, J_2s^1, SEM. **f** Pore-filling authigenic chlorite, well X20, 1613.19 m, J_2s^1, PPL

Table 4 Calculated salinity and temperature of different occurrences of calcite

Well	Depth (m)	Calcite occurrence	$\delta^{13}C_{PDB}$ (%)	$\delta^{18}O_{PDB}$ (%)	Z	S (‰)	T (C)
G30	2522.88	Replacement	−3.61	−15.23			74.87
G30	2547.65	Basal cementing	−3.19	−14.59	113.5	10.3	50.95
G36	2179.08	Basal cementing	−8.27	−13.87	103.5	11.5	58.48
G36	2184.01	Replacement	−19.84	−18.53			103.50
G36	2188.67	Replacement	−19.96	−19.31			111.38
G36	2193.75	Replacement	−19.87	−19.75			116.05
JP1	3287.06	Replacement	−20.98	−20.31			122.26
JP1	3288.06	Basal cementing	−19.01	−16.4	80.2	7.3	65.08
LQ009-H2	2618.69	Basal cementing	−26.08	−18.2	64.8	4.2	67.58
X20	1606.58	Replacement	−18.96	−18.73			105.47
X20	1613.69	Basal cementing	3.72	−17.36	126.3	5.6	58.48
X20	1615.87	Basal cementing	4.58	−16.4	128.5	7.3	71.19
Y2	2899.64	Basal cementing	−0.76	−13.49	119.0	12.2	42.30

the pore-lining chlorite (Fig. 6g, j), which shows that the quartz overgrowth formed almost simultaneously with the pore-lining chlorite. The leaf-shaped pore-filling chlorite covers the authigenic quartz in intergranular pores, which indicates that the pore-filling chlorite formed after pore-filling quartz (Fig. 6h). Authigenic quartz is mostly the product of precipitation of silicon ions released by the dissolution of feldspar particles, which implies that part of the pore-filling chlorite formed after the main dissolution period. The initial temperatures of quartz overgrowth were 60~70°C (Xi 2016), and the homogenization temperatures of fluid inclusions in the authigenic quartz filling fractures in the Sha 1 Member were 100~140 °C (Tao et al. 2015); the Ro of the source rock in the underlying Liangshan Formation generally ranges from 1.02 to 1.30%. These results show that the latest diagenetic stage experienced by the Sha 1 Member was phase A2 of mesodiagenesis. Therefore, combined with the classification standard of diagenetic stages of clastic rocks (2003), the diagenetic sequence of the study area and the main formation periods of chlorites with different occurrences are clarified (Fig. 8). The formation temperatures of grain-coating chlorite and inner pore-lining chlorite were less than 60°C, corresponding to phase A of eodiagenesis. The formation temperatures of the outer pore-lining chlorite ranged from 60 to 100°C, corresponding to phase B of eodiagenesis to phase A1 of mesodiagenesis, and the pore-filling chlorite was deposited at temperatures greater than 100°C, corresponding to phase A2 of mesodiagenesis.

Formation mechanism of authigenic chlorite

Grain-coating chlorite and inner pore-lining chlorite

The sandstones of the Sha 1 Member are mainly distributed in the delta front subfacies and chlorite/smectite (C/S) mixed-layer clay minerals are widespread. Therefore, the grain-coating chlorite and inner pore-lining chlorite mainly arose through two formation mechanisms as follows: (1) During the original period to phase A of eodiagenesis, large amounts of CO_2 and humic acid are released due to the transformation of organic matter to kerogen. Many plagioclase and biotite grains and magmatic rock fragments are strongly hydrolyzed and dissolved in the sandstones of the Sha 1 Member. During this process, large amounts of Na^+, Ca^{2+}, Mg^{2+}, Fe^{2+}, and Si^{4+} enter the pore fluid, which increases the salinity of the pore fluid and produces an alkaline fluid environment, and debris particles are mainly in suspension or point contact. Under these conditions, Mg^{2+} and Fe^{2+} in the pore fluid precipitate around the clastic particles to form grain-coating chlorite and inner pore-lining chlorite. (2) Montmorillonite transforms into chlorite. The montmorillonite carried into the lake by rivers forms a montmorillonite coating around the clastic particles. This montmorillonite coating is directly converted into chlorite in an alkaline diagenetic environment with abundant Fe^{2+} and Mg^{2+} fluid (Cao et al. 2018). However, the temperature and pressure are relatively low during phase A of eodiagenesis, and Fe^{2+} and Mg^{2+} ion hydration is strong. Under these conditions, it is difficult for these ions to enter the mineral crystal lattice (Parker and Sellwood 1983). Therefore, the grain-coating chlorite and inner pore-lining chlorite have poorly crystalline shapes and low Fe^{2+} and Mg^{2+} contents (Table 3).

Outer pore-lining chlorite

The pore-lining chlorite formed from phase B of eodiagenesis to phase A1 of mesodiagenesis (Fig. 8). During phase B of eodiagenesis, the organic matter is in an immature state, and the pore fluid remains alkaline. Various ions such as Ca^{2+}, Fe^{3+}, Fe^{2+}, and Mg^{2+}, are released into the pore fluid of the

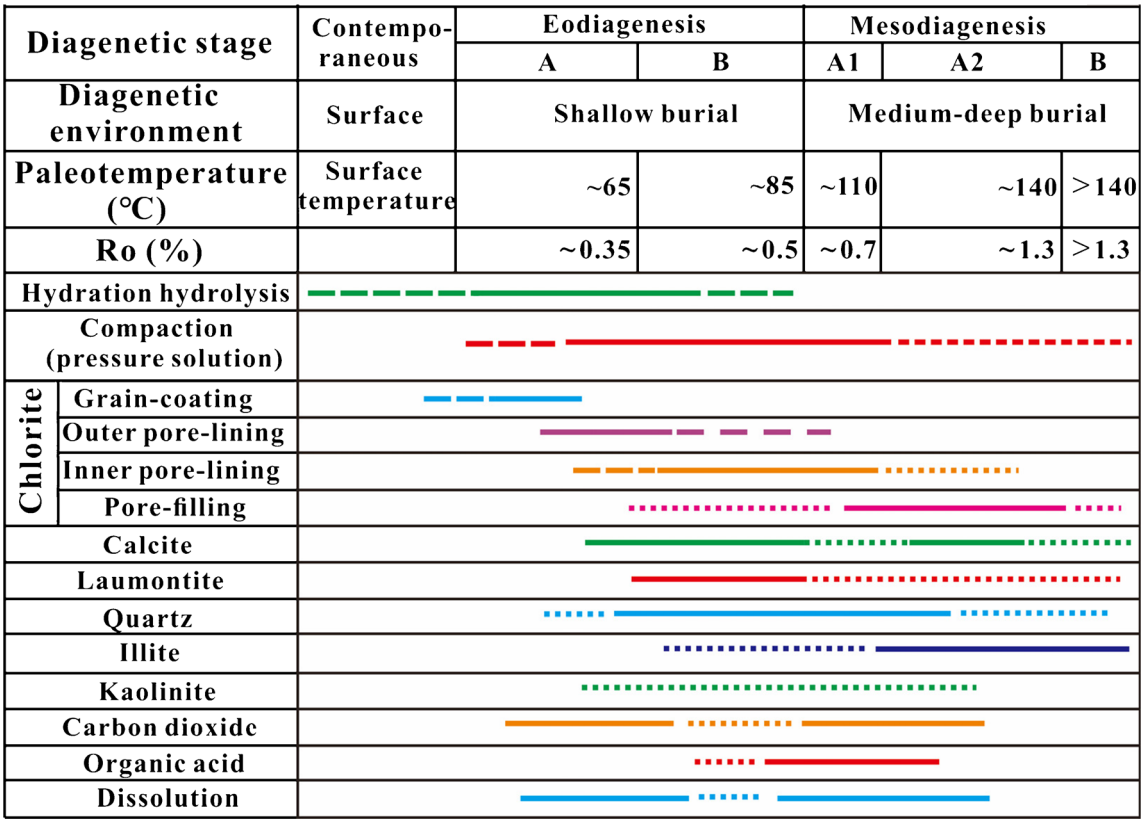

Fig. 8 Diagenetic evolution sequence of the Sha 1 Member

adjacent sandstones due to montmorillonite transforming to illite in the mudstone during phase A1 of mesodiagenesis, and large amounts of organic acids and carbonic acid are injected into the sandstones accompanied by hydrocarbon emplacement. Minerals such as feldspar and magmatic rock fragments and biotite are intensely dissolved and release various ions, such as Fe^{2+}, Mg^{2+}, and Si^{4+}. Therefore, these two processes provide sufficient sources for the formation of the outer pore-lining chlorite. With increasing burial temperature and pressure, the hydration strengths of Fe and Mg ions decrease significantly (Parker and Sellwood 1983), which is beneficial for chlorite formation. The feldspars (or rock fragments) covered by chlorite rims are dissolved, but the chlorite rims are not (Fig. 6b, i), which indicates that the acidic pore fluid is suitable for chlorite precipitation during phase A1 of mesodiagenesis. The causes of this phenomenon are as follows. (1) Under burial conditions, the Gibbs free energy increment of feldspar chloritization is less than 0 (Zhu et al. 1995). (2) The dissolution of silicate minerals reduces the acidity of pore fluids (Yuan et al. 2016). (3) Chlorite can precipitate in an acidic environment with a pH value as low as 5.7 (Haile et al. 2015). Therefore, with a suitable diagenetic

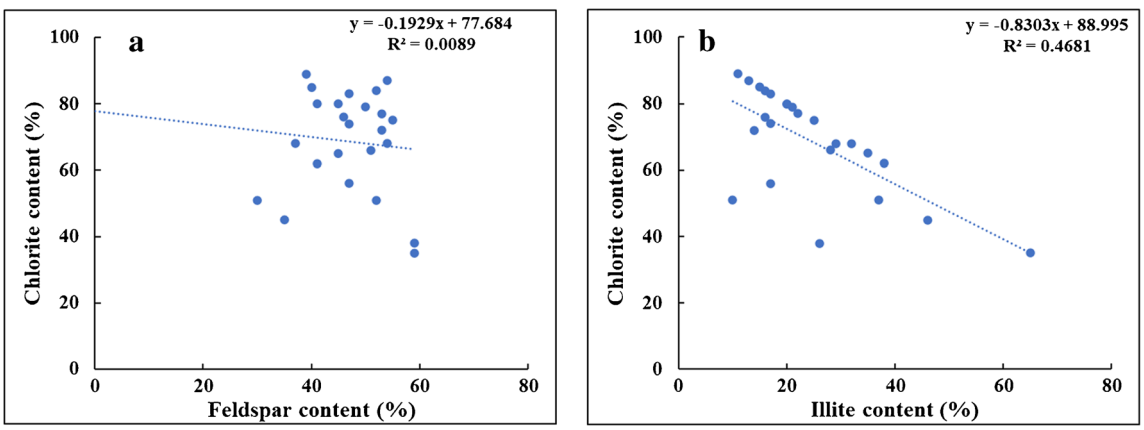

Fig. 9 **a** Correlation diagram of chlorite and feldspar. **b** Correlation diagram of chlorite and illite

Table 5 Chemical constituents of rocks related to chlorites

Rock types	Chemical composition (%)												
	SiO_2	Al_2O_3	Fe_2O_3	FeO	MgO	K_2O	Na_2O	CaO	TiO_2	MnO	P_2O_5	H_2O	CO_2
Granites in the provenance area of Sha 1 Member[a]	65.80	15.70	3.87	1.06	0.57	5.38	4.10	2.05	0.15	0.05			
Mudstone of Sha 1 Member in central Sichuan Basin[b]	63.27	17.00	5.21	0.72	1.78	2.96	1.52	1.11	0.76	0.05	0.16	4.51	0.12

Notes: a and b data are from Chen et al. (2018) and Wang et al. (2007), respectively

environment and sufficient material sources, chlorite can be continuously precipitated along the edges of pores to form pore-lining chlorite from phase B of eodiagenesis to phase A1 of mesodiagenesis. At this stage, the porosity and permeability of sandstone are high, and there is sufficient space for chlorite deposition, so the crystals of the outer pore-lining chlorite are complete and well developed. The growth process from the inner pore-lining chlorite to the outer pore-lining chlorite conforms to the Ostwald ripening law (Jahren 1991); therefore, the outer pore-lining chlorite is thicker.

Pore-filling chlorite

There are two formation mechanisms for pore-filling chlorite. (1) The formation mechanism is similar to that of the outer pore-lining chlorite. With large-scale decarboxylation of organic acids and the consumption of H^+ by dissolution of silicate minerals, the pore fluid gradually changes from acidic to alkaline during phase A1 of mesodiagenesis. Thus, the leaf-shaped and rose-shaped chlorites fill in the pores. (2) Clay mineral transformation. Kaolinite is very scarce in the Sha 1 Member, and the illite content is significantly negatively correlated with that of chlorite (Fig. 9b).

$3NaAlSi_3O_8(Albite) + K^+ + 2H^+ + H_2O = KAl_3Si_3O_{10}(OH)_2(Illite) + 3Na^+ + 6SiO_2 + H_2O$ (Eq.1) [Yuan et al. 2016]

$Illite + 1.64Mg^{2+} + 1.89Fe^{2+} + 8.24H_2O = 0.82Chlorite + 0.6K^+ + 1.37H_4SiO_4 + 6.46H^+$ (Eq. 2) [Kaiser 1984]

$3NaAlSi_3O_8$ (Albite) $+ 2Mg^{2+} + 2Fe^{2+} + 5H_2O = Fe_2Mg_2Al_3Si_2O_{10}(OH)_5$ (Chlorite) $+5H^+ + 7SiO_2 + 3Na^+$ (Eq. 3)

The reaction formula (Eq. 3) is modified from Morad and Aldahan (1987) and can be regarded as the addition reaction of feldspar dissolution into illite (Eq. 1) and illite chloritization (Eq. 2). The transformation from illite to chlorite is observed under a scanning electron microscope (Fig. 6k). Therefore, under temperature (>110°C) and high pressure, other clay minerals (such as illite) can transform to chlorite in pore fluids with sufficient Fe^{2+} and Mg^{2+} during phase A1 of mesodiagenesis. Due to the continued early mechanical compaction, dissolution, and clay mineral transformation, the sources of Fe^{2+} and Mg^{2+} significantly decrease during phase A2 of mesodiagenesis (Tian et al. 2008), and the porosity and permeability of the sandstone and the adjacent mudstone become quite low. The material transfer between sandstone and mudstone is very slow (Yang et al. 2016), so pore-filling chlorite rarely develops.

Authigenic chlorite formation pattern

The feldspar in the Sha 1 Member experienced intense dissolution (Fig. 6i). However, the correlation between the content of chlorite and that of feldspar is extremely poor (r=0.1; Fig. 9a), indicating that there were other material sources for chlorite. The sandstone of the Sha 1 Member is rich in felsic magmatic rock fragments (average 4.4%) and biotite. Felsic magmatic rock fragments (Table 5) and biotite can release many Fe and Mg ions during hydration, hydrolysis, and

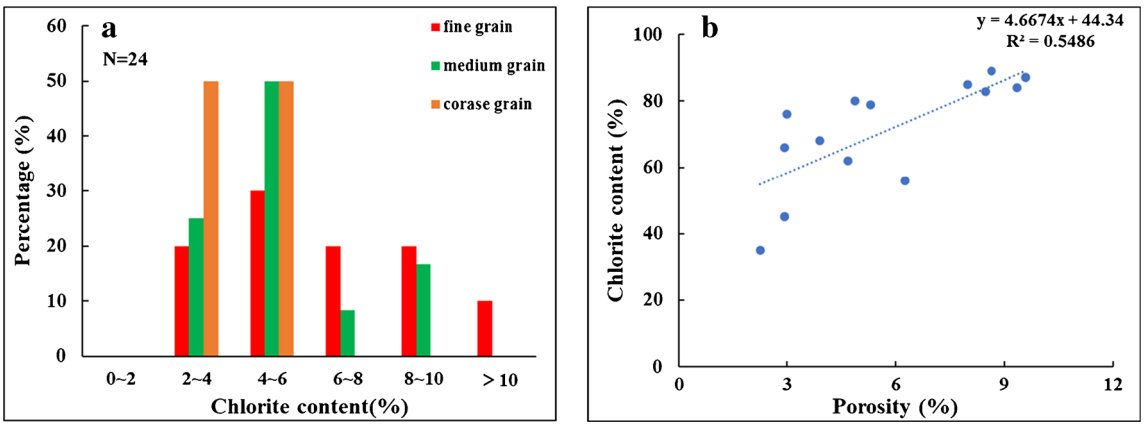

Fig. 10 **a** Distribution histogram of authigenic chlorites with different grain sizes. **b** Correlation diagram of chlorite and porosity

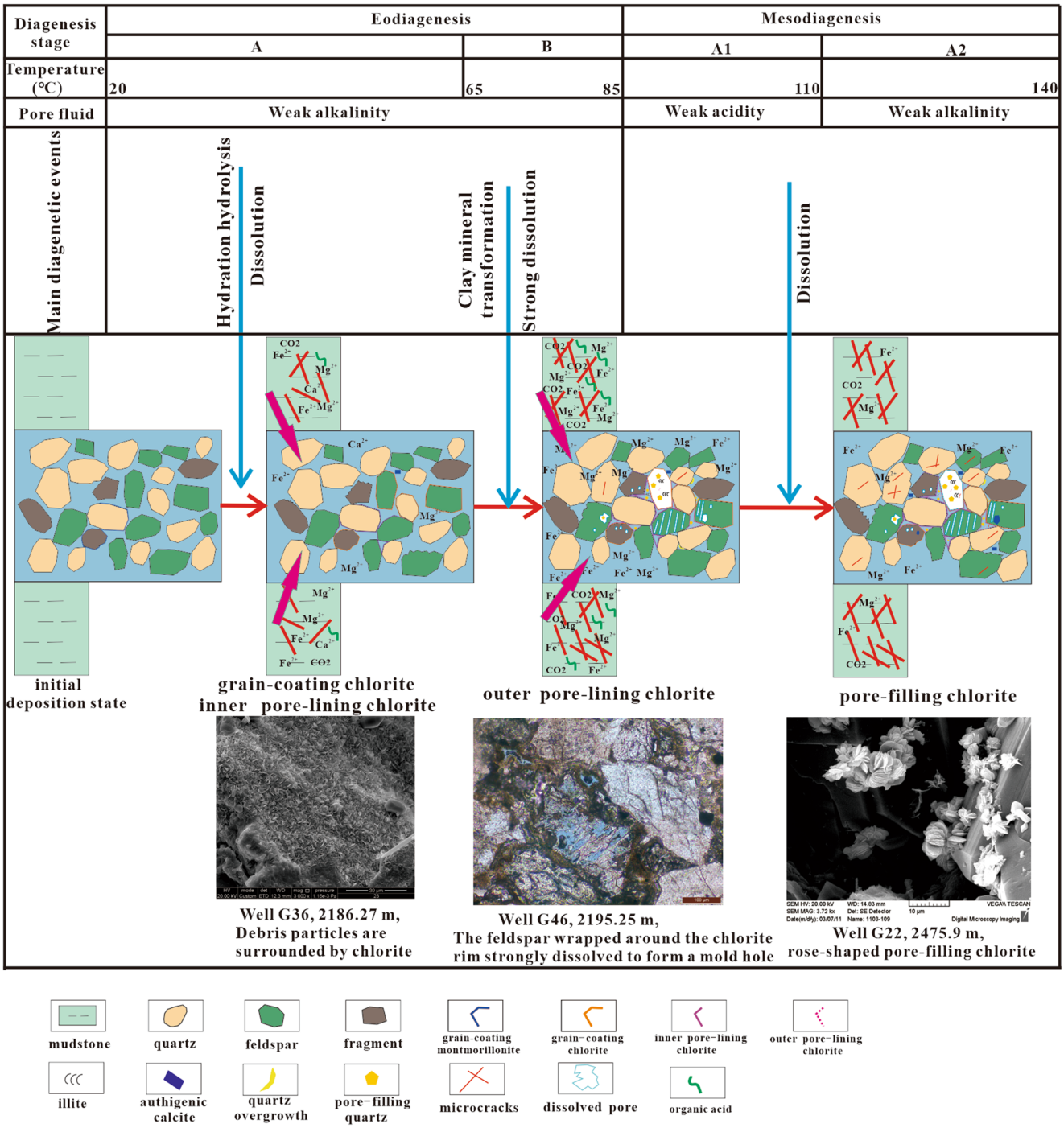

Fig. 11 Formation model of chlorite in the sandstone of the Sha 1 Member

dissolution. Fe and Mg contents in the mudstone of the Sha 1 Member are relatively high (Table 5). Due to the clay mineral transformation and the dissolution of silicate minerals by acidic fluids during organic matter maturation, the mudstone could release large numbers of Fe and Mg ions, which could enter the adjacent sandstones with migrating compaction fluid. The contents of Fe and Mg in the outer pore-lining chlorite and pore-filling chlorite are equivalent (Table 3), showing that the supply of Fe and Mg ions was sufficient during authigenic chlorite precipitation. The contents of chlorite and illite are significantly negatively correlated (r=0.68, Fig. 9b), which indicates that the pore fluids were more favorable for authigenic chlorite. The reason for this phenomenon is that K-feldspar contents are low in the sandstones of the Sha1 Member (Table 2) and the K in the mudstone mainly exists in illite (Iijima 2001). Therefore, K^+ in diagenetic fluids was low, but the supply of Fe and Mg ions was sufficient, which resulted in chlorite precipitation.

The authigenic chlorite mainly occurs in sandstones deposited in shallow lake beach bars, estuary sand bars, and underwater distributary channel microfacies. Authigenic chlorite is most developed in fine and medium sandstones, followed by coarse sandstone (Fig. 10a). The physical properties of sandstones developed in shallow lake beach bars, estuary sand bars, and underwater distributary channels are relatively good, which is favorable for chlorite development (Fig. 10b). The sandstone of the Sha 1 Member is mainly produced in the form of interlayers in thick mudstone (Fig. 2), which is conducive to the fluid in the mudstone carrying organic acids, CO_2, and Fe and Mg ions into the adjacent sandstones with better porosity and permeability.

Based on the analysis of the chlorite formation mechanism and main controlling factors, the formation modes of authigenic chlorite with different occurrences are established (Fig. 11)

Conclusions

(1) Authigenic chlorite was mainly produced in the form of pore-lining chlorite. Grain-coating chlorite and pore-filling chlorite are rare in the sandstones of the Sha 1 Member in the northeastern part of the central Sichuan Basin. Pore-lining chlorite has a double-layer structure and mainly formed in the early diagenetic stage.

(2) The grain-coating chlorite and inner pore-lining chlorite formed in phase A of eodiagenesis. Their formation was related to the direct precipitation of chlorite surrounding the particles and the conversion of terrestrial smectite coating to chlorite in pore fluids with sufficient Fe^{2+}, Mg^{2+}, and Si^{4+}. The outer pore-lining chlorite formed from phase B of eodiagenesis to phase A1 of mesodiagenesis. Its formation was closely related to the Fe^{2+} and Mg^{2+} provided by the conversion of montmorillonite to illite in the adjacent mudstone and the dissolution of silicate minerals by organic acids and carbonic acid. Pore-filling chlorite mainly formed in phase A2 of mesodiagenesis, which was related to the dissolution of silicate minerals by carbonic acid and the conversion of other minerals (such as illite) to chlorite.

(3) The material sources for authigenic chlorite were the dissolution of magmatic rock fragments and biotite grains and mudstone compaction fluid. Shallow lake beach bars, estuary sand bars, and underwater distributary channels were favorable sedimentary microfacies for chlorite development. The fine and medium sandstones adjacent to thick mudstone in the favorable facies belt were favorable locations for chlorite development.

Acknowledgements We thank the anonymous reviewers for their valuable suggestions and assistance in improving the quality of the manuscript and the Institute of Exploration and Development of PetroChina Southwest Oil & Gas field Company for sample collection and technical support.

Author contributions Conceptualization: Qinming Cao and Zhengxiang Lv. Methodology: Zhengxiang Lv. Formal analysis and investigation: Xiang Li and Yuanhua Qing. Writing—original draft preparation: Zhengxiang Lv. Writing—review and editing: Qinming Cao. Resources: Dong Huang. All authors have read and agreed to the published version of the manuscript.

Declarations

Conflict of interest The authors declare they have no conflicts of interest.

References

AliKhoudja SA, Chellat S, Hacini M, Semiani A (2020) Petrography and authigenic chlorite in the Siegenian reservoir rocks Berkine Basin eastern Algerian Sahara. Arab J Geosci 13:767–782

Alotaibi MB, Nasralla RA, Nasr-El-Din HA (2011) Wettability studies using low-salinity water in sandstone reservoirs. SPE. Res Eval Eng 14:713–725

Anjos SMC, De Ros LF, Silva CMA (2009) Chlorite authigenesis and porosity preservation in the upper Cretaceous marine sandstones of the Santos basin, offshore eastern Brazil. Clay Miner Sand 34:289–316

Bahlis AB, De Ros LF (2013) Origin and impact of authigenic chlorite in the Upper Cretaceous sandstone reservoirs of the Santos Basin, eastern Brazil. Pet Geosci 19:185–199

Branimir S, Giovanni Z, Andrea M (2020) On the origins of eogenetic chlorite in verdine facies sedimentary rocks from the Gabon Basin in West Africa. Mar Pet Geol 112:1–15

Cao Z, Liu GD, Meng W, Wang P, Yang CY (2018) Origin of different chlorite occurrences and their effects on tight clastic reservoir porosity. J Pet Sci Eng 160:384–392

Chen SJ, Wan MX, Du M, Zhang J, Xie BH (2005) Jurassic oil–gas source correlation and hydrocarbon source condition in central Sichuan region. Nat Gas Explor Dev 28:11–14 (in Chinese)

Chen XT, Xie QX, Qi W (2018) Study on the geochemical characteristics and tectonic environment of the Micangshan tectonic magmatic zone in the area of the Guangyuan city of Ying Chi. Sichuan Nonferrous Met 2018:11–13 (in Chinese)

Dowey PJ, Hodgson DM, Worden RH (2012) Pre-requisites, processes, and prediction of chlorite grain coatings in petroleum reservoirs: a review of subsurface examples. Mar Pet Geol 32:63–75

Ehrenberg SN (1993) Preservation of anomalously high porosity in deeply buried sandstones by grain-coating chlorite: examples from the Norwegian continental shelf. AAPG Bull 77:1260–1286

Gould K, Pe-piper G, Piper DJW (2010) Relationship of diagenetic chlorite rims to depositional facies in Lower Cretaceous reservoir sandstones of the Scotian basin. Sedimentology 57:587–610

Grigsby JD (2001) Origin and growth mechanism of authigenic chlorite in sandstones of the lower Vicksburg Formation, South Texas. J Sediment Res 71:654–656

Haile BG, Hellevang H, Aagaard P, Aagaard P, Jens J (2015) Experimental nucleation and growth of smectite and chlorite coatings on clean feldspar and quartz grain surfaces. Mar Pet Geol 68:664–674

Heald MT (1950) Authigenesis in West Virginia Sandstones. J Geol 58: 624–633

Heald MT, AndereggR C (1960) Differential cementation in the Tuscarora sandstone. J Sediment Res 30:568–577

Huang SJ, Xie LW, Zhang M, Wu WH, Shen LC, Liu J (2004) Formation mechanism of authigenic chlorite and relation to preservation of porosity in nonmarine Triassic reservoir sandstones, Ordos basin and Sichuan basin, China. J Chengdu Univ Tech (Sci & Techy Edi) 31:273–281(in Chinese)

Huggett JM, Burley SD, Longstaffe FJ, Saha S, Oates MJ (2015) The nature and origin of authigenic chlorite and related cements in Oligo-Miocene reservoir sandstones, Tapti gas fields, Surat depression, offshore western India. J Pet Geol 38:383–409

Iijima A (2001) Zeolites in petroleum and natural gas reservoirs. Rev Mineral Geochem 45:347–402

Jahren JS (1991) Evidence of Ostwald ripening related recrystallization of diagenetic chlorites from reservoir rocks offshore Norway. Clay Miner 26:169–178

Kaiser WR (1984) Predicting reservoir quality and diagenetic history in the Frio formation (Oligocene) of Texas. AAPG Mem 37:195–216

Keith ML, Weber JN (1964) Carbon and oxygen isotopic composition of selected limestones and fossils. Geochim Cosmochim Acta 28: 1787–1816

Lan YF (2011) Influences of authigenic chlorites on sandstone reservoir quality in Chang-8 member of the Upper Triassic Yanchang formation in Jiyuan-Huaqing area, Ordos basin. Dissertation, Chengdu University of Technology (in Chinese)

Li W, Qin SF (2012) Characteristics of trace elements and hydrogen and oxygen isotopes in the formation water of the Xujiahe formation, Sichuan basin. Acta Pet Sin 33:55–63 (in Chinese)

Li ZS, Li XC, Ma CH, Li JY, Zhang ZH, Gao X, Zhang WL, Xu CL (2008) Analysis method for carbon and oxygen isotope in organic matter and carbonate. National Energy Administration, Beijing (in Chinese)

Lin YT, Pan ZR (2001) Study on density and torming dassification of gas field brine. J Salt Lake Res 9:1–7

Line LH, Jahren J, Hellevang H (2018) Mechanical compaction in chlorite-coated sandstone reservoirs- examples from Middle-Late Triassic channels in the southwestern Barents sea. Mar Pet Geol 96:48–370

Liu JK, Peng J, Liu JJ, Wang Y, Liu JF (2009) Pore-preserving mechanism of chlorite rims in tight sandstone-an example from the T_3x formation of Baojie area in the transitional zone from the central to southern Sichuan basin. Oil Gas Geol 3:53–58

Mahmoud E, Mohamed AN (2018) Effect of chlorite clay-mineral dissolution on the improved oil recovery from sandstone rocks during diethylenetriaminepentaacetic acid chelating-agent flooding. SPE J 23:1880–1898

Morad S, Aldahan A (1987) Diagenetic chloritization of feldspars in sandstones. Sediment Geol 51:155–164

Parker A, Sellwood BW (1983) Sediment diagenesis. Bjørlykke K. Diagenetic reactions in sandstones, Springer, Dordrecht

Pittman ED, Lumsden DN (1968) Relationship between chlorite coatings on quartz grains and porosity, Spiro Sand, Oklahoma. J Sediment Res 38:668–670

Pittman ED, Larese RE, Heald MT (1992) Clay coats: occurrence and relevance to preservation of porosity in sandstones. SEPM Spec Publ 47:241–255

Ren YG, Wang C, Wu HB, Yu J, Shao HM, Wang ZM, Wang GS, Guo HL (2011) Evaluating methods of oil and gas reservoirs. National Energy Administration, Beijing (in Chinese)

Sun ZX, Sun ZL, Yao J, Wu ML, Liu JR, Dou Z, Pei CR (2014) Porosity preservation due to authigenic chlorite coatings in deeply buried upper Triassic Xujiahe formation sandstones, Sichuan basin, Western China (Article). J Pet Geol 37:251–267

Tao SZ, Yang YM, Pang ZL, Yang G, Yang JJ, Yang XP, Wu YY, Zhang TS (2015) The fluid inclusion characteristics and formation, evolution of tight oil of Jurassic, Sichuan basin. Acta Petrol Sin 31: 1089–1100 (in Chinese)

Tian JF, Chen ZL, Fan YF, Li PP, Song LJ (2008) The occurrence, growth mechanism and distribution of authigenic chlorite in sandstone. Bull. Mineralo Petrol Geoche 27:00–207 (in Chinese)

Virolle M, Brigaud B, Luby S, Portier E, Fenies H, Bourillot R, Patrier P, Beaufort D (2019) Influence of sedimentation and detrital clay grain coats on chloritized sandstone reservoir qualities: insights from comparisons between ancient tidal heterolithic sandstones and a modern estuarine system. Mar Pet Geol 107:163–184

Wang QW, Liang B, Kan ZZ (2007) Geochemistry and implications for the source areas and weathering in the Shaximiao formation, Zigong, Sichuan. Sediment Geol Tethyan Geol 27:17–21

Warren J (2000) Dolomite: occurrence, evolution and economically important associations. Earth-Sci Rev 52:1–81

Worden RH, Griffiths J, Wooldridge LJ, Utley JEP (2020) Lawan AY. Muhammed DD, Simon N, Armitage PJ

Xi KL (2016) Genetic mechanism of tight sandstone oil and gas reservoir of the Cretaceous Quantou formation fourth member in the southern Songliao basin, China. Dissertation, China University of Petroleum (East China) (in Chinese)

Xia H, Perez EH, Dunn TL (2020) The impact of grain-coating chlorite on the effective porosity of sandstones (Article). Mar Pet Geol 115: 1–12

Xiang F, Wang YW, Feng Q, Zhang DY, Zhao JX (2016) Further research on chlorite rims in sandstones: evidence from the Triassic Yanchang formation in the Ordos basin, China. Arab J Geosci 9: 507–508

Xie WR, Yang W, Zhao XY, Wei GQ, Xie ZY, Jin H, Chen G (2010) Influences of chlorite on reservoir physical properties of the Xujiahe formation in the central part of Sichuan basin. Pet Explor Dev 37: 74–679

Yang YM, Yang JJ, Yang G, Tao SZ, Ni C, Zhang B, He XD, Lin JP, Huang D, Liu M, Zou J (2016) New research progress of Jurassic tight oil in central Sichuan basin. Pet Explor Dev 43:873–882

Yin G, Ni SJ (2009) Isotope geochemistry. Geological Publishing House, Beijing, p 87

Yuan GH, Cao YC, Wang YZ (2016) Dissolution mechanism and its impact on physical properties of feldspar and carbonate minerals in clastic reservoirs. Petroleum Industry Press, Beijing, pp 235–239(in Chinese).

Zhang W (2013) The evolution of the ancient lake and tight oil reservoirs formation of the early and middle Jurassic in the NE part of central Sichuan basin. Dissertation, Chengdu University of Technology (in Chinese)

Zhao YG, Wang M, Jiang YQ, Dong ZX, Wang SR (2010) Diagenesis of the low-permeability sandstone reservoir of the first member of Shaximiao formation in Gongshanmiao area and its influence on the reservoir property. J Xi'An Pet Univ (Nat Sci Edi) 25:7–22 (in Chinese)

Zhou QS, Lv CF, Li C, Chen GJ, Ma XF, Li CZ (2020) Formation mechanism of authigenic chlorite in tight sandstone and its influence on tight oil adsorption, Triassic Ordos basin, China. Energy Explor Exploit 38:2667–2694

Zhu JX, Li SZ, Zhu JW (1995) Study on diagenetic system of super-deep wells. Tongji University Press, Shanghai, pp 64–78